Nuclear Instruments and Methods in Physics Research B 349 (2015) 64–71

Contents lists available at ScienceDirect

Nuclear Instruments and Methods in Physics Research B

journal homepage: www.elsevier.com/locate/nimb

# New method to evaluate the $^{7}Li(p,n)^{7}Be$ reaction near threshold

María S. Herrera [a,b,c,*], Gustavo A. Moreno [d,e], Andrés J. Kreiner [a,b,c]

[a] Comisión Nacional de Energía Atómica, Av. Gral. Paz 1499, Buenos Aires B1650KNA, Argentina
[b] Consejo Nacional de Investigaciones Científicas y Técnicas, Av. Rivadavia 1917, Ciudad Autónoma de Buenos Aires C1033AAJ, Argentina
[c] Escuela de Ciencia y Tecnología, UNSAM, 25 de Mayo y Francia, Buenos Aires B1650KNA, Argentina
[d] YPF Tecnología, Baradero S/N, Buenos Aires 1925, Argentina
[e] Departamento de Física J. J. Giambiagi, Facultad de Ciencias Exactas y Naturales, UBA, Ciudad Universitaria, Ciudad Autónoma de Buenos Aires 1428, Argentina

ARTICLE INFO

*Article history:*
Received 6 April 2013
Received in revised form 3 January 2015
Accepted 19 January 2015
Available online 27 February 2015

*Keywords:*
$^{7}Li(p,n)^{7}Be$ reaction near threshold
Cross section
Neutron yield
Accelerator-based neutron source
Boron Neutron Capture Therapy (BNCT)

ABSTRACT

In this work a complete description of the $^{7}Li(p,n)^{7}Be$ reaction near threshold is given using center-of-mass and relative coordinates. It is shown that this standard approach, not used before in this context, leads to a simple mathematical representation which gives easy access to all relevant quantities in the reaction and allows a precise numerical implementation. It also allows in a simple way to include proton beam-energy spread affects. The method, implemented as a C++ code, was validated both with numerical and experimental data finding a good agreement. This tool is also used here to analyze scattered published measurements such as (p,n) cross sections, differential and total neutron yields for thick targets. Using these data we derive a consistent set of parameters to evaluate neutron production near threshold. Sensitivity of the results to data uncertainty and the possibility of incorporating new measurements are also discussed.



## 1. Introduction

Many potential applications of neutron sources have motivated recently the increase in research and development for accelerator based devices which are of particular interest in the treatment of high grade malignant tumors using Boron Neutron Capture Therapy (BNCT) [1–3]. The development of accelerators, capable of delivering high intensity proton beams, is not trivial but within reach of present day technology. Appropriate proton-induced nuclear reactions can be used to produce the neutron spectra required for this therapy modality. In particular, the endothermic $^{7}Li(p,n)^{7}Be$ nuclear reaction near threshold can be used to produce low-energy neutrons with a forward-peaked distribution in the laboratory system which is suitable for BNCT [4–10]. As it is well known the ground state *Q*-value of the reaction is −1644.24 keV with a threshold value given by a proton energy of 1880.57 keV yielding neutrons with 29.68 keV close to the desirable epithermal energy range useful in most of BNCT tumor targets [11–13].

Kinematical calculations including the relativistic correction with numerical and graphical representations can be made using different on-line calculators. However, these programs may have some limitations and do not give the possibility to manipulate the variables for computing the accelerator-based neutron source necessary for any Monte Carlo simulation. These is the reason for which researchers have been developing different codes that produces yield data for the $^{7}Li(p,n)$ nuclear reaction near-threshold. In 1999 Lee and Zhou [14,15] published a code for computing thick target differential neutron yields from monoenergetic proton beams near-threshold. The kinematical non-relativistic calculations are based on a two-body interaction in the laboratory frame. The use of this reference frame brings with it multiple branches in the calculation and some associated numerical problems. DROSG2000 package [16] (first release in 1987 where some nuclear reactions were available) indeed, produces yield data of 59 monoenergetic accelerator-based neutron sources using relativistic expressions. However, in particular for the $^{7}Li(p,n)$-reaction near threshold, an unbounded behavior in the differential neutron yield at 0° occurs. In 2008 a new Monte-Carlo based program namely PINO (Protons In Neutrons Out), was developed to estimate the neutron spectra during activation experiments [17]. According to Reifarth et al. in PINO the emission angle and energy are randomly acquired based on the double differential cross-section compiled by Liskien and Paulsen [18] fulfilling momentum and energy conservation laws. It should be pointed out that according to Shorin [19] "A certain problem with the experimental data arose after publication of Ref. [20] in 1966, in which the graphic data of a number of works were tabulated. In the process, errors were made in the determination of the energy scale amounting to −1.35 keV

* Corresponding author at: Comisión Nacional de Energía Atómica, Av. Gral. Paz 1499, Buenos Aires B1650KNA, Argentina.
*E-mail address:* herrera@tandar.cnea.gov.ar (M.S. Herrera).

http://dx.doi.org/10.1016/j.nimb.2015.01.080
0168-583X/

for the data of Refs. [21–24] which proved very important in the region around the threshold. The data in Ref. [20] were automatically included in Ref. [18]". Care should be taken if this data is used in the calculation. On the basis of the cross section formula and the values given in Ref. [18], a correction was performed by Shorin to the values in the threshold energy region.

The computational tool SimLiT [25] (also a Monte-Carlo based program) is similar to that developed by Reifarth et al. but allows higher simulation statistics and addresses in a different way critical issues of energy dependence of the cross-section just above threshold and proton statistics. However, the calculation shows some sensitivity near threshold leading a small dip in the spectrum at 28 keV approximately (See Fig. 5 in [25]). Recently in 2014, a new calculation based on the binary collision approximation (BCA) method, or the detailed Monte Carlo technique, was published to study the D-T and p-$^7$Li neutron sources [26]. In particular for the $^7$Li(p,n)$^7$Be nuclear reaction, the program has a numerical bug to get $E_{th}$. As a result a "well" appears at the neutron energy around 30 keV (see Fig. 9 in [26]).

In this work, we consider a new method to evaluate the $^7$Li(p,n)$^7$Be reaction near threshold based on the parameterization of the p-$^7$Li reaction using center-of-mass (CM) and relative coordinates. The method allows to compute not only the differential neutron yield but also to give a more practical way to calculate all the relevant quantities involved in this reaction avoiding all the singularities. The proposed numerical implementation (here coded in C++) allows a straightforward analysis of the problem where the relevant quantities are calculated independently by simple functions. Using this method we review most (if not all) of the available experimental neutron data near threshold including cross section and differential, integrated and total neutron yields. These data sets are compared and analyzed finding a consistent description of the neutron source and giving new insight for possible strategies to enhance the value of future measurements via sensitivity analysis.

## 2. Center-of-mass and relative coordinate kinematical approach

In this work we parametrize the kinematic variables involved in the $^7$Li(p,n)$^7$Be nuclear reaction by the center-of-mass and relative coordinates. The new parameterization proposed in the present work makes it easy to manipulate the kinematical quantities in the reaction via simple functions and, as it will be shown below, this parameterization is useful not only to compute the kinematics back in the laboratory reference frame but also to calculate the differential neutron yield for thick targets including a proton energy spread effect, improving the previous numerical codes.

It should be pointed out that an exact description of the reaction can be given via relativistic energy and momentum conservation (as in Ref. [16]) however, in the energy range considered in this work we can use a newtonian approximation for the linear momentum and kinetic energy with a relative error below $10^{-3}$. For example, the small corrections associated to a fully relativistic calculation lead to threshold of 1880.57 keV (and 1880.30 keV when the approximation is made).

In order to clarify our notation let us call $E_n$ and $\theta_n$ the energy and emission angle of the neutron in LR and $E_p$ the incident proton energy in such frame. Instead of using the neutron emission angle in LR, $\theta_n$, we parametrize the output using $\Theta_n$, the neutron angle in a reference system at rest in the >center-of-mass of the products. An invertible mapping

$$E_n = E_n(E_p, \Theta_n)$$
$$\theta_n = \theta_n(E_p, \Theta_n)$$

will be established using momentum and energy conservation. In what follows the pair of coordinates $(E_p, \Theta_n)$ will be used to derive all the quantities of interest and the inversion back to the LR will be invoked when needed. Note that the angle $\Theta_n$ is in principle a variable in the range $[0, \pi]$ that will have a certain probability distribution according to the specific form of the nuclear reaction cross section (low energy processes for example will result in a uniform distribution). When the incident proton energy is equal to the minimum energy required to produce the reaction given by 1880.3 keV. In this case the neutron is at rest in the center-of-mass of the products giving a LR energy of 29.68 keV. Nuclear masses employed were calculated using the 2003 mass evaluation [27] neglecting the electron binding energies.

Considering the momentum conservation, it is easy to obtain together with a Galileo transformation the neutron velocity in LR which explicitly define $\vec{v}_n(E_p, \Theta_n)$. The calculation is completed when the neutron final state is determined in terms of $E_p$ and $\Theta_n$. Of course, any quantity of interest such as $E_n$ and $\theta_n$ can be calculated based on the center-of-mass approach. For example, Fig. 1 depicts the variation of the neutron emission angle in LR for different proton energies as a function of the angle in the final center-of-mass frame. This clearly shows that an energy $E_p^*$ exists for which the maximum emission angle is limited below $\pi/2$. Unlike Lee and Zhou program where some difficulties may arise at or close to the maximum emission lab angle, using the attached numerical implementation in C++ the maximum values for each proton energy can be easily extracted. These maximum values are shown in Fig. 2 as a function of the incident proton energy. Other quantities of interest are the maximum and minimum neutron energies in LR as a function of the incident proton energy. These values can be trivially obtained as $E_n^{min} = E_n(E_p, \pi)$ and $E_n^{max} = E_n(E_p, 0)$, as it is shown in Fig. 3, where the neutron energy range is plotted as function of the incident proton energy. Moreover, in the figure it is included different lines that separate the same number of particles, in this case 10 % of the neutrons are contained within each interval of adjacent lines. This plot is useful to understand the neutron energy spread as a function of incident proton energy. In particular it shows that the number of high energy neutrons is relatively low and most of the neutrons are concentrated at energies near threshold. Typically, when the incident energy is above 1.96 MeV there is a clear trend to larger energy values. Similar ideas can be applied to the angular distribution of particles.

Fig. 4 depicts the energy integrated cross section per unit angle $dN/d\Theta_n$ (that is $\int_0^\pi d\Theta_n\, dN/d\Theta_n = 1$) in a polar plot. The angular

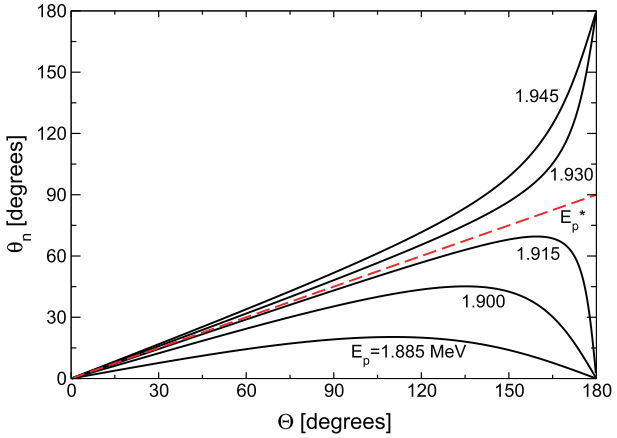


**Fig. 1.** Laboratory neutron angle vs. CM neutron angle. Note that when the proton energy is lower than $E_p^* = 1.92$ MeV exist maximum LR angles for each proton energy contour.

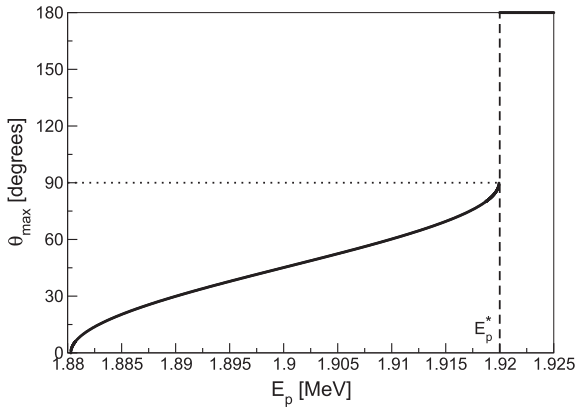


**Fig. 2.** Maximum laboratory neutron emission angle as a function of the proton energy. Above $E_p^*$ all angles are permitted.

distribution is not very sensitive to the incident energy and is typically centered around 30° (maximum probability in the polar plot goes from 22° for 1.90 MeV to 36° at 2.00 MeV).

Other ranges not near threshold can be calculated in a similar fashion using this technique.

Despite the fact that we use the $(E_p, \Theta_n)$ coordinates in the calculation, it should be stressed that no generality is lost because the mapping $(E_p, \Theta_n) \rightarrow (E_n, \theta_n)$ can be univocally inverted. This calculation is explicitly shown in the appendix and succinctly coded into the supplementary files of this publication. As will be shown in the following section the center-of-mass and relative coordinate kinematical approach will be useful to calculate the double differential neutron yield for thick lithium targets in a straightforward manner.

## 3. Neutron yield calculation based on the center-of-mass and relative coordinates approach

The calculation of the neutron yield based on the parameterization of the kinematic quantities using the center-of-mass and relative coordinates is described in this section. In particular this method can be used to compute the angular and energy distributions of neutrons near threshold. The formalism for computing the differential neutron yield for the $^7$Li(p,n) reaction was previously proposed by Ritchie in 1976 [28] and later used by others authors [14,15,29–31]. It is characterized by

$$\frac{d^2N}{dE_n\, d\Omega}(E_n, \theta_n) = \frac{f_{^7Li} N_0}{e A_{eff}} \frac{1}{S(E_p)} \frac{d\sigma}{d\Omega^{CM}} \frac{d\Omega^{CM}}{d\Omega} \frac{\partial E_p}{\partial E_n}\bigg|_{\theta_n} \quad (1)$$

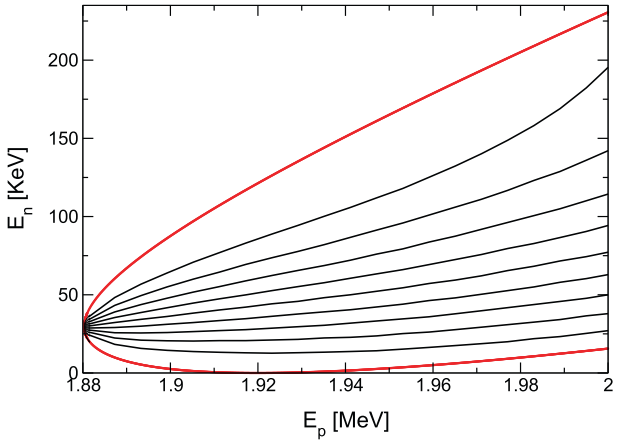


**Fig. 3.** Neutron energy as a function of the incident proton energy. Intermediate lines separate the total number of particles in fractions of 10 %.

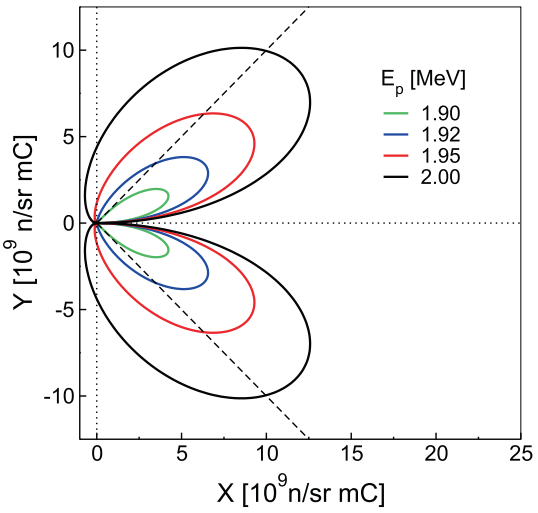


**Fig. 4.** Neutron angular distribution $dN/d\Theta_n$ (polar-plot) for different proton energies. Black dashed lines represent ± 45°.

where $f_{^7Li}$ is the $^7$Li atomic fraction of natural lithium (0.925), $N_0$ is Avogadro's number, $e$ is the electronic charge, $A_{eff}$ is the effective atomic weight of natural lithium and $S(E_p)$ is the proton mass stopping power in lithium. In this expression $d\Omega^{CM}/d\Omega$ is the Jacobian factor between solid angles (CM and LR) and $\partial E_p/\partial E_n$ accounts for the neutron energy interval generated by proton energy loss in the material. The variables in $d^2N/dE_n\, d\Omega$ are $(E_n, \theta_n)$ and thus it is implicitly assumed that non-zero values correspond to beam energies above $E_p(E_n, \theta_n)$. In particular, the stopping power function $S(E_p)$ has to be evaluated via $E_p := E_p(E_n, \theta_n)$. Eq. (1) already takes into account the sum of all contributions from protons with energies in the range $E_{th}$ to the incident beam energy. Eq. (1) also applies to semi-thick targets, in such case non-zero values correspond to a region where there exist solutions to $E_p^{in} \geqslant E_p(E_n, \theta_n) \geqslant E_p^{out}$ with $E_p^{in}$ and $E_p^{out}$ the input and output proton energies on the slab of material.

Lee and Zhou's algorithm uses Eq. (1) for the computation of the angular and energy distributions of neutrons. Their method is based on the use of the variables $E_n$ and $\theta_n$ in LR, that is, for each point $(E_n, \theta_n)$ they calculate the proton energy using an analytical expression and some intermediate parameters defined previously by Winter and Schmid in 1968 [32]. Then they work out the Jacobian products of Eq. (1) which they need to handle all together to avoid some computational problems for values of $(E_n, \theta_n)$ at or close to the maximum emission lab angle however, no reasons are given in their paper. Lee and Zhou also remark that there is another difficulty near threshold where $\frac{d\Omega^{CM}}{d\Omega}\frac{dE_p}{dE_n} \rightarrow \infty$, because one of the parameters in their method is unbounded when $E_p$ is close to the threshold value. As we shall see in what follows, using the CM parameterization in Eq. (1), yields a simple way to identify and remove singularities, however using our proposed method no singularity will be found at or close to the maximum emission lab angle as in Lee and Zhou's procedure. In particular it will be shown that only when $\sin(\theta_n) \rightarrow 0$ a removable singularity appears, which can be circumvented taking a limit by extrapolation without having to use a specific analytical form for the model $d\sigma/d\Omega^{CM}$ (See also Section 4 for the discussion on this quantity).

The neutron yield in our scheme can be coupled to the kinematical analysis to obtain quantities that can be calculated in any of the two coordinate systems (LR or CM) by simple function calls, which allows a more flexible framework to manipulate the quantities in the problem.

To derive the conversion of Eq. (1) to CM variables first note that

$$\frac{d\sigma}{d\Omega}(E_p,\theta_n)d\Omega = \frac{d\sigma}{d\Omega^{CM}}(E_p,\Theta_n)d\Omega^{CM} \tag{2}$$

which implies that

$$\frac{d\sigma}{d\Omega}(E_p,\theta_n) = \frac{d\sigma}{d\Omega^{CM}}(E_p,\Theta_n)\left[\frac{\sin(\Theta_n)}{\sin(\theta_n)}\frac{1}{\frac{\partial\theta_n}{\partial\Theta_n}\Big|_{E_p}}\right]. \tag{3}$$

Then the double differential neutron production takes the form

$$\frac{d^2N}{dE_n\,d\Omega} = \frac{f_{^7Li}N_0}{eA_{eff}}\frac{1}{S(E_p)}\frac{\partial E_p}{\partial E_n}\Big|_{\theta_n}\frac{d\sigma}{d\Omega^{CM}}(E_p,\Theta_n)\left[\frac{\sin(\Theta_n)}{\sin(\theta_n)\frac{\partial\theta_n}{\partial\Theta_n}\Big|_{E_p}}\right]. \tag{4}$$

The only quantity that remains to be transformed in the Eq. (4) to the set of variables $(E_p,\Theta_n)$ is $\partial E_p/\partial E_n|_{\theta_n}$, but for fixed $\theta_n$ (that is $\delta\theta_n = 0$) one has the relations

$$\begin{cases} 0 &= \frac{\partial\theta_n}{\partial\Theta_n}\Big|_{E_p}\delta\Theta_n + \frac{\partial\theta_n}{\partial E_p}\Big|_{\Theta_n}\delta E_p \\ \delta E_n &= \frac{\partial E_n}{\partial\Theta_n}\Big|_{E_p}\delta\Theta_n + \frac{\partial E_n}{\partial E_p}\Big|_{\Theta_n}\delta E_p \end{cases} \tag{5}$$

therefore

$$\delta E_n|_{\theta_n} = \left(\frac{\partial E_n}{\partial\Theta_n}\Big|_{E_p}\left(-\frac{\frac{\partial\theta_n}{\partial E_p}\Big|_{\Theta_n}}{\frac{\partial\theta_n}{\partial\Theta_n}\Big|_{E_p}}\right) + \frac{\partial E_n}{\partial E_p}\Big|_{\Theta_n}\right)\delta E_p|_{\theta_n} \tag{6}$$

yielding

$$\frac{\partial E_p}{\partial E_n}\Big|_{\theta_n} = \frac{\frac{\partial\theta_n}{\partial\Theta_n}}{\frac{\partial E_n}{\partial E_p}\frac{\partial\theta_n}{\partial\Theta_n} - \frac{\partial E_n}{\partial\Theta_n}\frac{\partial\theta_n}{\partial E_p}}. \tag{7}$$

In this way we have

$$\frac{d^2N}{dE_n\,d\Omega}(E_p,\Theta_n) = \frac{f_{^7Li}N_0}{eA_{eff}}\frac{1}{S(E_p)}\frac{d\sigma}{d\Omega^{CM}}(E_p,\Theta_n) \times\left[\frac{1}{\frac{\partial E_n}{\partial E_p}\frac{\partial\theta_n}{\partial\Theta_n} - \frac{\partial E_n}{\partial\Theta_n}\frac{\partial\theta_n}{\partial E_p}}\right]\left[\frac{\sin(\Theta_n)}{\sin(\theta_n)}\right] \tag{8}$$

where $E_n = E_n(E_p,\Theta_n)$ considering

$$\vec{v}_n = \left(\frac{\sqrt{2m_pE_p}}{M_f} + \frac{m_{Be}}{M_f}v_f\cos(\Theta_n)\right)\hat{x} + \left(\frac{m_{Be}}{M_f}v_f\sin(\Theta_n)\right)\hat{y}, \tag{9}$$

in $E_n(E_p,\Theta_n) = \frac{1}{2}m_n\left(v_{n,x}^2(E_p,\Theta_n) + v_{n,y}^2(E_p,\Theta_n)\right)$. The neutron angle in LR is the unique solution in $[0,\pi]$ of the system

$$|\vec{v}_n|\cos(\theta_n) = v_{n,x}(E_p,\Theta_n) \tag{10}$$

$$|\vec{v}_n|\sin(\theta_n) = v_{n,y}(E_p,\Theta_n), \tag{11}$$

defining univocally $\theta_n = \theta_n(E_p,\Theta_n)$. Eq. (8) explicitly allows to calculate $d^2N/dE_n\,d\Omega$ as a function of $(E_p,\Theta_n)$, furthermore, exploiting the mapping $(E_p,\Theta_n)\leftrightarrow(E_n,\theta_n)$ one can also evaluate $d^2N/dE_n\,d\Omega$ as a function of $(E_n,\theta_n)$ by simple composition of functions. In our procedure for computing the double differential neutron yield near threshold (for example for an incident proton beam of 1.910 MeV) only the values of $E_n$ and $\theta_n$ that satisfy 1.910 MeV $\geqslant E_p(E_n,\theta_n)$ will be allowed producing a surface with a sharp boundary shown in Fig. 5 thus, increasing the incident energy only increases the accessible region without changing the shape of the surface as can be seen in the Fig. 6 where a top view of the double differential yield and the lines that separate different incident proton energies are shown. However, if a proton energy spread is included in the calculation, for example through a gaussian energy distribution with a standard deviation of 6 keV, the boundary of Fig. 5 changes as shown in Fig. 7. The possibility of including a probability model in the double differential cross section calculation is a simple exercise and has been included in the code provided with this manuscript.

Eq. (8) shows where the calculation of the differential neutron yield may have instabilities. Derivatives in equation are calculated numerically in our code using centered finite differences. The numerical difficulties can only appear when the determinant of the transformation

$$d = \frac{\partial E_n}{\partial E_p}\frac{\partial\theta_n}{\partial\Theta_n} - \frac{\partial E_n}{\partial\Theta_n}\frac{\partial\theta_n}{\partial E_p} \tag{12}$$

approaches zero or when $\sin(\theta_n)\to 0$. The condition $d = 0$ implies a singularity in the mapping $(E_p,\Theta_n)\leftrightarrow(E_n,\theta_n)$, which occurs only at the threshold energy $E_p = E_p^{th}$ for any $\Theta_n$ or at $E_p = E_p^*$ for $\Theta_n = \pi$ (see Fig. 1). The case where $E_p = E_p^*$ at $\Theta_n = \pi$ is a soft removable singularity that does not generate problems for the purpose of this work because the numerical truncation at $\theta_n = \pi/2$ renders it finite. In contrast, the singularity at $E_p = E_p^{th}$ only gives a finite result when multiplied by the CM cross section.

The other case to be analyzed involves the limit $\sin(\theta_n)\to 0$ which, as it can be seen from Fig. 1, is no more than a removable singularity because the ratio $\sin(\Theta_n)/\sin(\theta_n)$ is always convergent as $\sin(\theta_n)\to 0$ (note that for these cases $E_p\neq E_p^{th}$ and $E_p\neq E_p^*$). This removable singularity can also be handled by extrapolation. The threshold point is included in the latter case, thus both limits are solved with the same extrapolation procedure. In practice, our implementation extrapolates these values with a quadratic Lagrange polynomial and values of $\theta_n$ in the range $[0, 0.15]$ degrees, which give a maximum deviation of 0.08 % for neutrons in a range of 0.05 keV around the threshold. This maximum deviation decays rapidly away from threshold, for example it goes below 0.001 % in the next 0.05 keV. When $\theta\to\pi$ the double differential cross section is very flat and the limit can be estimated using the value $\theta = \pi - 10^{-5}$ with a relative error below $10^{-5}$ %.

Moreover, using the code attached with this manuscript it is easy to show that a finite result can only be found if

$$\lim_{E_p\to E_p^{th}}\frac{\frac{d\sigma}{d\Omega^{CM}}(E_p,\Theta_n)}{\sqrt{E_p - E_p^{th}}} < \infty. \tag{13}$$

That is, the CM cross section model must behave as $\sqrt{E_p - E_p^{th}}$ for $E_p$ near threshold to obtain a finite (non-zero) neutron yield. Note that this behavior is a consequence of energy and momentum conservation only. In the following section the theoretical model discussed satisfies this condition and thus the singularity can be easily removed taking the numerical limit.

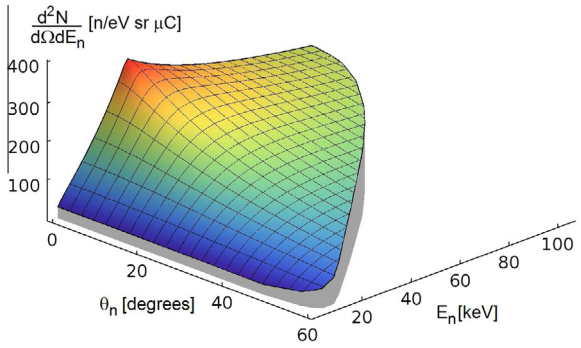


**Fig. 5.** Double differential neutron yield for $E_p = 1.910$ MeV incident protons on a natural thick lithium target.

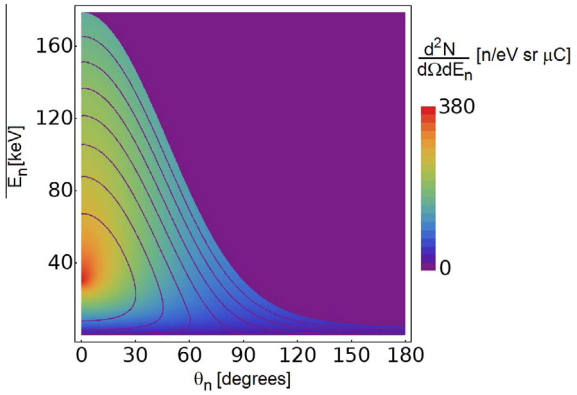


**Fig. 6.** Double differential neutron yield (colors) as function of emission angle and neutron energy for different incident proton energies on natural thick lithium target. Higher values of the incident proton beam energy broaden the accessible region. Here energies of $(1.89 + 0.01\,n)$ MeV with $n$ an integer in the range $n \in [0, 7]$ are shown. (For interpretation of the references to color in this figure legend, the reader is referred to the web version of this article.)

## 4. Differential cross section model, experimental data and discussion

An evaluation of the available total cross-section data until 1994 of the $^{7}$Li(p,n) reaction in the proton energy region up to 2 MeV was performed by Shorin [19]. In his article the theoretical formula described previously in Refs. [21,22,24] of the total cross section $\sigma_{(p,n)}$ near threshold in the center-of-mass system is analyzed together with the channel widths of the reaction, the possible contributions to the spins of the $J$ and $T$ states, and the inverse (n,p)-reaction, increasing the complexity in the formula.

The simplest way to describe the differential cross section needed in Eq. (8) is to use the reduced Breit–Wigner (B–W) formula given by

$$\frac{d\sigma}{d\Omega^{CM}}(E_p) = \lambda\!\!\!^{-2}_{p}\, g(J)\, \frac{\Gamma_n/\Gamma_p}{(1+\Gamma_n/\Gamma_p)^2}, \tag{14}$$

where it was assumed that $|E_p - E_r| \ll \Gamma/2$ and that the CM differential cross section is not directionally dependent in the proton energy range of $[E_p^{th}, 1.93]$ MeV. Here $\Gamma$ is the sum of the proton and neutron widths, $\Gamma_p$ and $\Gamma_n$ respectively, $E_r$ is the resonance energy in CM and $g(J) = 5/8$ is the statistical factor that measures the probability that a particular compound nucleus will form according to the total spin of the projectile and the target nucleus [21]. The reduced de Broglie wavelength for the relative coordinate, $\bar{\lambda}_p$, can be calculated as

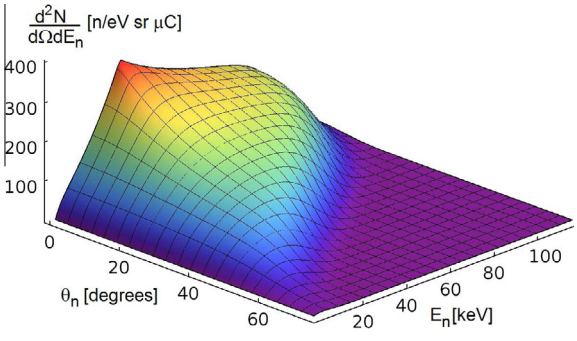


**Fig. 7.** Double differential neutron yield for $E_p = 1.910$ MeV incident protons with an assumed standard deviation of $\sigma = 6$ keV on a natural thick lithium target.

$$\lambda\!\!\!^{-2}_{p} = \frac{\hbar^2 (m_p + m_{Li})^2}{2\, m_p\, m_{Li}^2}\, \frac{1}{E_p}, \tag{15}$$

thus, evaluating the pre factor in Eq. (14) and considering the energy dependence of the particle channel widths as $x \equiv \Gamma_n/\Gamma_p \approx C\sqrt{1 - E_p^{th}/E_p}$ [24], the only parameter that has to be fitted from experimental data is $C$. We review and analyze most (if not all) available experimental neutron data near threshold such as the (p,n) cross section, differential, integrated and total neutron yields reported by different authors searching for a consistent calibration of this parameter.

Experimental data of the (p,n) cross section near threshold as function of proton energy in LR is shown in Fig. 8 together with the evaluated ENDF/B-VII.1 library [33]. In the figure, the original data points were divided by $4\pi$ to obtain the differential cross section $d\sigma/d\Omega^{CM}$. Although the most recent measurements of the (p,n) cross section reaction near threshold were taken by Sekharan et al. in 1977 [34], the older experimental data obtained between 1957 and 1959 by Newson et al. [21], Macklin et al. [22] and Gibbons et al. [23] was used to calculate the dimensionless parameter $C$. For the purpose of this work the Sekharan data was disregarded since the authors reported that the data near threshold "is expected to be more nearly correct" in the older experiments because of a weaker dependence of the neutron energy detector efficiency near threshold.

The best fit (least-squares) of the analytical formula to the selected data is obtained when $C = 3.60 \pm 0.25$ however, this value is different from that reported by Lee and Zhou when applying the B-W formula to Gibbons' data [15]. In their procedure the value $C$ was fixed to $C = 6$ and the pre-factor in Eq. (14), namely in their work $A$, (which can be calculated *a priori*, given a vale of 169.72 MeV mb/sr) was adjusted. The resulting fit using the parameters reported by Lee ($A = 164.913$ MeV mb/sr and $C = 6$) is acceptable in the flat region, but does not reproduce properly the initial rise of the data. It should be pointed out that neither Lee's fit nor the best fit presented in this work can reproduce the correct concavity in the reported data.

However, there exists another observable that can be used to corroborate the prediction of Eq. (14), and eventually fit $C$ using our method to evaluate the $^{7}$Li(p,n)$^{7}$Be reaction near threshold. In particular combining Eq. (14) with the double differential neutron yield of Eq. (8) one can compute the double differential neutron yield at $\theta_n = 0°$ with $C$ as a fitting parameter. In our

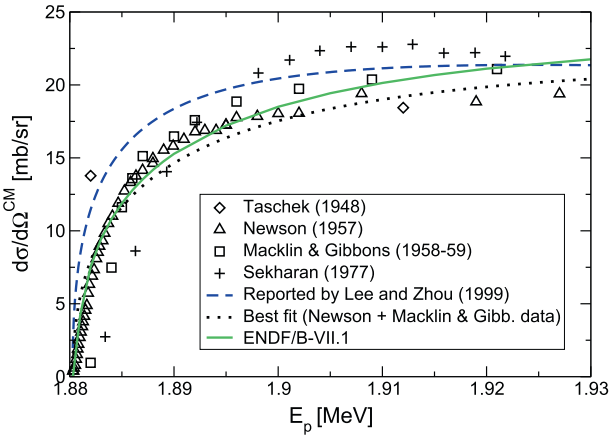


**Fig. 8.** Differential (p,n) cross section data near threshold as function of proton energy in the laboratory frame. Original experimental data points and the were divided by $4\pi$. The dashed line is calculated using parameters reported by Lee and Zhou [15] and the dotted line is the best fit to the data using Eq. (14).

implementation each quantity was coded into an independent function, thus it results easy to use the code to obtain a least squares fit of the 0° data to estimate the value. Measurements by Kononov et al. in 1977 [31] are a good test for the analytical model. For the purpose of computing the differential neutron yield, the stopping power values of protons on lithium from SRIM [35] were used. In this analysis we distinguish two different data sets, S1 and S2. S1 corresponds to all experimental data points shown in Fig. 9, while S2 contains a subset of S1, without measurements in the neutron energy interval [25.75, 44] keV. The set S2 is generated to avoid any possible deviation to smaller values near threshold due to the proton energy spread, and to compare the sensitivity of the fit to those data-points. Using these sets the values obtained for $C$ by least squares fit were $C_{S1} = (5.82 \pm 0.05)$ and $C_{S2} = (6.00 \pm 0.05)$, assuming an independent gaussian noise for the deviations. Both estimations and, moreover, the curve computed with Lee's program represent fairly well the differential yield data of Kononov. It should be noted that the experimental data shown in Fig. 9 is not compatible with that shown in Fig. 8, because the best fit to Newson's and Macklin & Gibbons' data generates a differential neutron yield at zero degree (Fig. 9) that is far below Kononov's findings (and viceversa, using the best fit with the Kononov's data, the cross section is almost the same as the curve shown in Fig. 8 with Lee's parameters).

The deviations associated to the best fit of Newson-Gibbons data are also seen in the total neutron yield reported by other publications. The total neutron yields have been measured by different authors in the range $[E_{th}, 1.93]$ MeV [5,15,36,37]. Both ours and Lee's calculations are compatible with the deviations reported in the experimental data, however, important differences between curves using Kononov's or Newson's and Macklin & Gibbons' data are found (Fig. 10). Since the values published by Yu et al. [36] are two times lower than those obtained by other authors and no reasons causing this difference were reported, these data was disregarded in Fig. 10. Moreover, analyzing different observables such as the double differential neutron yield, neutron energy spectrum and angular distributions it was found that the zero-angle double differential neutron yield is the observable with maximum sensitivity to the parameter $C$. Thus Kononov's measurement impose stringent conditions on this variable. Taking into account the latter observation and the fact that these measurements are compatible with other quantities measured by many other authors, we find

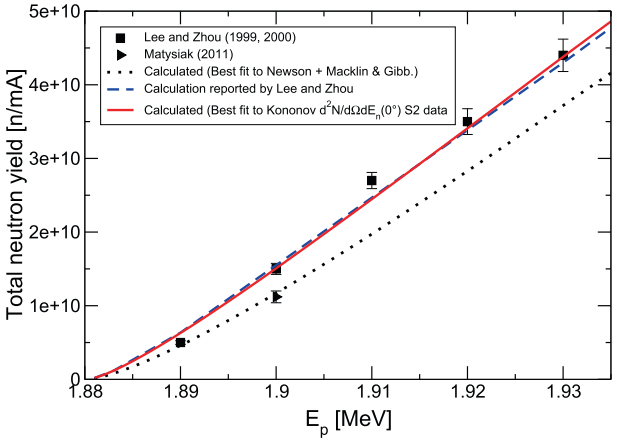


**Fig. 10.** Experimental values of total neutron yields for protons on natural lithium metal reported by different authors. Computed neutron yields using different sets of data for the theoretical cross section are also shown.

Kononov data to be the most appropriate for a calibration of the analytical formula near threshold.

Neutron spectrum at different angles and neutron energy spectra measurements were published by Feinberg et al. [38] and Lederer et al. [39] in 2012. Neutrons produced by the $^7$Li(p,n)$^7$Be reaction at the mentioned proton energy were used for nuclear astrophysics to study the quasistellar neutron spectrum for a thermal energy of around 25–30 keV [39–41]. Since the reported data was given in arbitrary units we used these measurements to test the spectrum shape. In particular, Fig. 11 depicts the neutron spectrum at $0 \pm 2.9°$ obtained with a proton energy of $1912 \pm 1.5$ keV. Calculations were compare to the experimental results of Feinberg et al. considering a standard deviation of $\sigma = 1.5$ keV and using both $C = 3.6$ and $C = 6$ parameters derived from the different data sets (Gibbons and Kononov, respectively). The first value of $C$ was derived adjusting the differential cross section model described in Section 4 to Gibbons' data. The second value was obtained adjusting the double differential neutron yield Eq. (8) to Kononov's data with $C$ as a fitting parameter. When the model with $C = 3.6$ is used, the calculation cannot reproduce Feinberg data. This could imply that either the model or the data (or both) are not correct. However when the model is used with the parameter $C = 6$, the data is fitted reasonably well. Since the experimental neutron

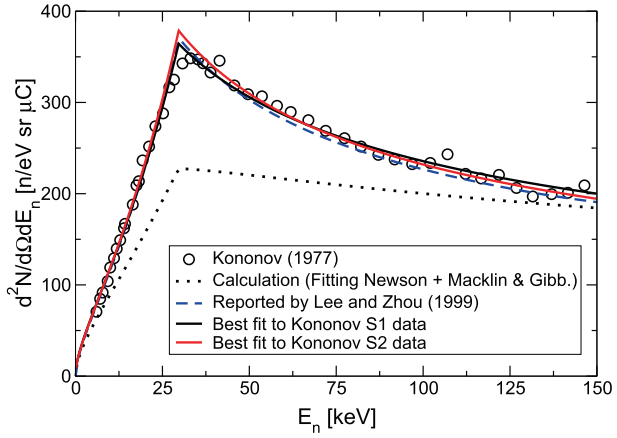


**Fig. 9.** Double differential neutron yield at zero degree as a function of neutron energy in the laboratory system (Kononov et al. [31]). Solid lines are best fits to Eq. (14) using this data (see the text for the meaning of S1 and S2). The differential neutron yield calculation reported by Lee and Zhou (dashed line) and calculated using Newson's and Macklin & Gibbons' data (dotted line) are also shown.

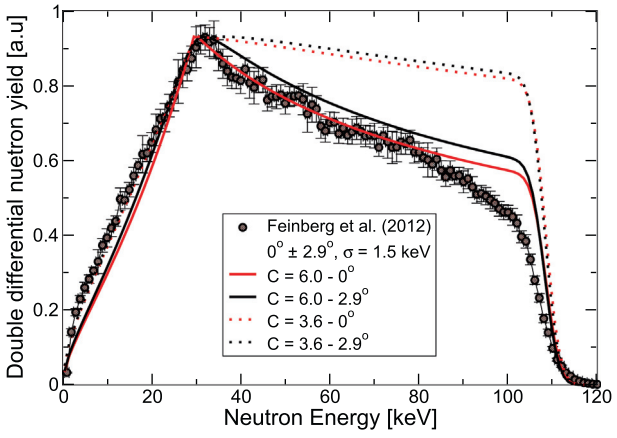


**Fig. 11.** Neutron spectrum at $0 \pm 2.9°$ at incident proton energy of $1912 \pm 1.5$ keV (Feinberg et al.) [38]. Theoretical curves with a standard deviation of $\sigma = 1.5$ keV were calculated using two values of parameter $C$, derived from the different data sets (Newson + Macklin & Gibbons and Kononov (1957), respectively).

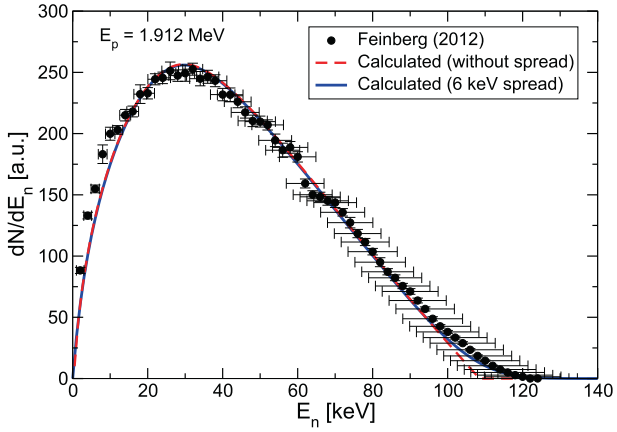


**Fig. 12.** Neutron energy spectrum as a function of measured neutron energy in the laboratory system (Feinberg et al.) [38]. Theoretical curves without proton energy spread and with a standard deviation of $\sigma = 6$ keV are also shown. Both calculated spectrums were derived from Kononov's best fit using the S2 data set ($C = 6$).

emission angle published by Feinberg is $0 \pm 2.9^\circ$ we calculated both angles, considering the reported energy spread of 1.5 keV. These behaviors (the wrong and good fits for 3.6 and 6, respectively) were obtained not only at zero degree but also in al experimental angles reported by Feinberg ($10, 20, 30^\circ, \ldots$). Our conclusion is that he differential cross section model in CM with $C = 6$ can be used in the calculation of the double differential neutron yield for the purposes of obtain an accelerator-based neutron source.

The second comparison was made considering the neutron energy spectra ($dN/dE_n$) with a narrow energy-spread of $\sigma = 6$ keV. As can be seen in Fig. 12 the shape of the neutron spectrum obtained in our numerical calculation is within the experimental errors of the measurements in all cases but when the proton energy spread is included the shape of the spectrum is improved in particular in the region of higher energies. All calculated neutron spectra were generated using the best fit to Kononov-S2 data to compute $C$ (that is $C = 6$) and a least squares fit to fix the amplitude in the range [0, 90] keV (data above 90 keV was not included in the fit because of its large uncertainties). These recent experimental results do also agree with the previous analysis, however as was the case for the total yield this observable is not so sensitive to the parameter $C$.

## 5. Summary and conclusions

In this work we have presented a new method based on center-of-mass and relative coordinates to describe the $^7$Li(p,n)$^7$Be reaction near threshold. The resulting numerical scheme is implemented in a C++ code that allows the calculation of any kinematical quantity in the process by simple function calls. Using this method we analyze most (if not all) available measurements to obtain a consistent description of the double differential neutron yield for accelerator-based neutron sources. This approach provides new insight on the sensitivity of neutron production to the parameters in the nuclear reaction model, giving also an efficient tool to fit numerical predictions to experimental data sets. In particular we have shown that the differential yield of neutrons reported by Kononov et al. [31] is the most sensitive curve when a Breit–Wigner formula is assumed to describe the threshold process in the proton energy range of $[E_p^{th}, 1.93]$ MeV. The best fit to this data was compared with integrated and total neutron yields showing a good agreement with other authors.

When proton energies are above 1.93 MeV, corrections to the differential cross section that account for non-isotropy become progressively important. Liskien and Paulsen [18] have measured the coefficients of the Legendre-polynomial expansion which give moderate corrections in the $E_p \in [1.93, 2]$ MeV range. Measurements in this range are not so abundant as the data sets discussed in the latter section and do only include two points per polynomial coefficient, which are used here (via interpolation) to account for deviations of the isotropic cross section in the CM frame. Again these modifications can be included in the calculation by simply adding terms in the CM cross section function, which is decoupled and easily accessible in our code. As was shown in this work the present code is a flexible approach that allows one to incorporate different data-sets and test the associated predictions. Since the code was written in a few lines using only independent functions both kinematical calculations and neutron yield production including the proton energy spread effects can be derived within the same program.

## Acknowledgement

The authors are grateful to Sara J. González and Javier Praena for useful discussions and to Oleg E. Kononov for providing theoretical data included in the validation of the code. This work was supported by the National Research Council of Argentina (CONICET).

## Appendix A. Inversion of mapping $(E_p, \Theta_n) \to (E_n, \theta_n)$

To invert the relation $(E_p, \Theta_n) \to (E_n, \theta_n)$ note that

$$v_{n,x} = v_n \cos(\theta_n) = \sqrt{\frac{2m_p E_p}{M_f}} + \frac{m_{Be}}{M_f} v_f(E_p) \cos(\Theta_n) \tag{A.1}$$

$$v_{n,y} = v_n \sin(\theta_n) = \frac{m_{Be}}{M_f} v_f(E_p) \sin(\Theta_n), \tag{A.2}$$

where $v_n = \sqrt{2E_n/m_n}$ and

$$v_f(E_p) = \sqrt{\frac{2\mu_i}{\mu_f}} \sqrt{\frac{E_p}{m_p} + \frac{m_p(M_f - M_i)}{\mu_i M_i M_f} E_p - \frac{|Q|}{\mu_i}}. \tag{A.3}$$

Thus it is straightforward to obtain a quadratic equation for $\sqrt{E_p}$ of the form

$$aE_p + b\sqrt{E_p} + c = 0, \tag{A.4}$$

where the coefficients $a, b$ and $c$ are given by

$$\begin{cases} a &= 2\left(\frac{m_{Be}}{M_f}\right)^2 \frac{\mu_i}{\mu_f m_p}\left(1 + \frac{m_p^2}{M_i \mu_i}\left(1 - \frac{M_i}{M_f}\right)\right) - \frac{2m_p}{M_f^2} \\ b &= 2\, v_{n,x} \frac{\sqrt{2m_p}}{M_f} \\ c &= -\left(v_{n,x}^2 + v_{n,y}^2 + \left(\frac{m_{Be}}{M_f}\right)^2 \frac{2|Q|}{\mu_f}\right). \end{cases} \tag{A.5}$$

It is easy to show that there exists only one positive root which defines unambiguously $E_p(E_n, \theta_n)$. Using this expression in Eqs. (A.1) and (A.2) one can find a unique $\Theta_p(E_n, \theta_n) \in [0, \pi]$ solving simultaneously for $\cos(\Theta_n)$ and $\sin(\Theta_n)$, which completes the inverse mapping $(E_n, \theta_n) \to (E_p, \Theta_n)$.

## Appendix B. Supplementary data

Supplementary data associated with this article can be found, in the online version, at http://dx.doi.org/10.1016/j.nimb.2015.01.080.

## References


[1] Y. Kiyanagi, K. Asano, A. Arakawa, S. Fukuchi, F. Hiraga, K. Kimura, H. Kobayishi, M. Kubota, H. Kumada, H. Matsumoto, A. Matsumoto, T. Sakae, K. Saito, T. Sahibata, M. Yoshioka, A project of boron neutron capture therapy system based on a proton linac neutron source, Phys. Procedia 26 (2012) 223–230.

[2] H. Tanaka, Y. Sakurai, M. Suzuki, S. Masunaga, Y. Kinashi, G. Kashino, Y. Liu, T. Mitsumoto, S. Yajima, H. Tsutsui, A. Maruhashi, K. Ono, Characteristics comparison between a cyclotron-based neutron source and KUR-HWNIF for boron neutron capture therapy, Nucl. Instrum. Methods Phys. Res. B 267 (2009) 1970–1977.

[3] A.J. Kreiner, W. Castell, H. Di Paolo, M. Baldo, J. Bergueiro, A.A. Burlon, D. Cartelli, V. Thatar Vento, J.M. Kesque, J. Erhardt, J.C. Ilardo, A.A. Valda, M.E. Debray, H.R. Somacal, J.C. Suarez Sandin, M. Igarzabal, H. Huck, L. Estrada, M. Repetto, M. Obligado, J. Padulo, D.M. Minsky, M.S. Herrera, S.J. Gonzalez, M.E. Capoulat, Development of a tandem-electrostatic-quadrupole facility for accelerator-based boron neutron capture therapy, Appl. Radiat. Isotopes 69 (2011) 1672–1675.

[4] X.-L. Zhou, C. Lee, F. Harmon, R. Hamm, Analysis of epithermal neutron production by near- threshold (p,n) reactions, Appl. Radiat. Isotopes 48 (1997) 1571–1575.

[5] C.L. Lee, X.-L. Zhou, R.J. Kudchadker, F. Harmon, Y.D. Harker, A Monte Carlo dosimetry-based evaluation of the 7Li(p,n)7Be reaction near threshold for accelerator boron neutron capture therapy, Med. Phys. 27 (1) (2000) 192–202.

[6] T. Kenichi, K. Tooru, S. Yoshinori, N. Yoshinobu, I. Masayori, H. Masaharu, Irradiation characteristics of BNCT using near-threshold 7Li(p,n)7Be direct neutrons: application to intra-operative BNCT for malignant brain tumours, Phys. Med. Biol. 47 (2002) 3011–3032.

[7] O.E. Kononov, V.N. Kononov, N.A. Solovev, Neutron source for Boron Neutron Capture Therapy based on the reaction 7Li(p,n)7Be near threshold, At. Energy 94 (6) (2003) 417–420.

[8] G. Bengua, T. Kobayashi, K. Tanaka, Y. Nakagawa, H. Unesaki, TPD-based evaluation of near threshold mono-energetic proton energies for the 7Li(p,n)7Be production of neutrons for BNCT, Phys. Med. Biol. 51 (2006) 4095–4109.

[9] S. Halfon, M. Paul, D. Steinberg, A. Nagler, A. Arenshtam, D. Kijel, I. Polacheck, M. Srebnik, High power accelerator-based boron neutron capture with a liquid lithium target and new applications to treatment of infectious diseases, Appl. Radiat. Isotopes 67 (2009) S278–S281.

[10] T. Kobayashi, G. Bengua, K. Tanaka, N. Hayashizaki, T. Katabuchi, T. Hattori, M. Aritomi, A novel BNCT irradiation system with an on-line monitor using 7Li(p,n)7Be near threshold neutrons, Radiat. Meas. 46 (12) (2011) 2000–2002.

[11] J.C. Yanch, X.-L. Zhou, G.L. Brownell, A Monte Carlo investigation of the dosimetric properties of monoenergetic neutron beams for neutron capture therapy, Radiat. Res. 126 (1) (1991) 1–20.

[12] E. Bisceglie, P. Colangelo, N. Colonna, P. Santorelli, V. Variale, On the optimal energy of epithermal neutron beams for bnct, Phys. Med. Biol. 45 (2000) 49–58.

[13] M.S. Herrera, S.J. González, D.M. Minsky, A.J. Kreiner, Evaluation of performance of an accelerator-based BNCT facility for the treatment of different tumour targets, Phys. Med. 29 (12) (2013) 436–446.

[14] C.L. Lee, X.-L. Zhou, An algorithm for computing thick target differential p-Li neutron yields near threshold, in: J.L. Duggan, I.L. Morgan (Eds.), Applications of Accelerators in Research and Industry, AIP, 1999, pp. 227–230.

[15] C.L. Lee, X.-L. Zhou, Thick target neutron yield for the 7Li(p,n)7Be reaction near threshold, Nucl. Instrum. Methods B 152 (1999) 1–11.

[16] M. Drosg. DROSG-2000, Codes and Data base for 59 Neutron Source Reactions, Documented in the IAEA Report IAEA-NDS-87 Rev. 9 (May), Received from the IAEA Nuclear Data Section.

[17] R. Reifarth, M. Heil, F. Käppeler, R. Plag, PINO – a tool for simulating neutron spectra resulting from the 7Li(p,n) reaction, Nucl. Instrum. Methods A 608 (2009) 139–143.

[18] H. Liskien, A. Paulsen, A 1975 neutron production cross-sections and energies for the reactions 7Li(p,n)7Be and 7Li(p,n)7Be, At. Data Nucl. Data Tables 15 (1975) 57–84.

[19] V.S. Shorin. Cross-section of the reaction 7Li(p,n)7Be close to the threshold. www.nds.iaea.org/publications/indc/indcccp0403.pdf (1997) 55–65.

[20] H.J. Kim, W.T. Milner, F.K. McGowan. Nucl. Data Tables, 1966, v.AL p. 203.

[21] H.W. Newson, R.M. Williamson, K.W. Jones, J.H. Gibbons, H. Marshak, Li7(p,n), (p, p′$\gamma$), and (p,$\gamma$) Reactions near Neutron Threshold, Phys. Rev. 108 (5) (1957) 1294–1300.

[22] R.L. Macklin, J.H. Gibbons, Phys. Rev. 109 (1) (1958) 105–109.

[23] J.H. Gibbons, R.L. Macklin, Phys. Rev. 114 (2) (1959) 571–580.

[24] J.H. Gibbons, H.W. Newson, Fast neutron physics, part I, in: J.B. Marion, J.L Fowler (Eds.), Interscience, New York, 1960, pp. 133–176.

[25] M. Friedman et al., Nucl. Instrum. Methods A 698 (2013) 117–126.

[26] G. Wang et al., Neutron characterization study for D-T, p-7Li neutron sources with new BCA based direct collision coupling method, Nucl. Instrum. Methods Phys. Res. A 757 (2014) 40–47.

[27] G. Audi, A.H. Wapstra, C. Thibault, The Ame, Atomic mass evaluation (II), Nucl. Phys. A 729 (2003) (2003) 337–676.

[28] A.I.M. Ritchie, Neutron yields and energy spectra from the thick target Li(p,n) source, J. Phys. D 9 (1976) 15–26.

[29] J.W. Meadows. Determination of the Energy Scale for Neutron Cross-section Measurements Employing a Monoenergetic Accelerator. ANL/TDM-25 (1977).

[30] W.V. Aslam, F.E. Prestwich, McNeill, Lithium target performance evaluation for low-energy accelerator-based in vivo measurements using gamma spectroscopy, Appl. Radiat. Isotopes 58 (2003) 321–331.

[31] V.N. Kononov, E.D. Poletaev, B.D. Yurlov, Absolute yield and spectrum of neutrons from the 7Li(p,n)7Be reaction, Atomnaya Energiya vol. 43 (4) (1977) 303–305.

[32] J. Winter, H. Schmid, EUR (1968) 3908e.

[33] M.B. Chadwick et al., Nuclear Data Sheets 112 (2011) 2887–2996.

[34] K.K. Sekharan, H. Laumber, B.D. Kern, F. Gabbard, A neutron detector for measurement of total neutron production cross sections, Nucl. Instrum. Methods 133 (1976) 253–257.

[35] J.F. Ziegler, Handbook of Stopping Cross-Sections for Energetic Ions in all Elements, vol. 5, Pergamon Press, New York, 1980. b0180.

[36] W. Yu, G. Yue, X. Han, J. Chen, B. Tian, Measurements of the neutron yields from 7Li(p,n)7Be reaction thick target with incident energies from 1.885 to 2.0 MeV, Med. Phys. 25 (7) (1998) 1222–1224.

[37] W. Matysiak, W.V. Prestwich, S.H. Byun, Precise measurements of the thick target neutron yields of the 7Li(p,n) reaction, Nucl. Instrum. Methods A 643 (2011) 47–52.

[38] G. Feinberg, M. Friedman, A. Krása, A. Shor, Y. Eisen, D. Berkovits, D. Cohen, G. Giorginis, T. Hirsh, M. Paul, A.J.M. Plompen, E. Tsuk, Quasi-stellar neutrons from the 7Li(p,n)7Be reaction with an energy-broadened proton beam, Phys. Rev. C 85 (5) (2012). 055810-1-12.

[39] C. Lederer, F. Käppeler, M. Mosconi, R. Nolte, M. Heil, R. Reifarth, S. Schmidt, I. Dillmann, U. Giesen, A. Mengoni, A. Wallner, Definition of a standard neutron field with the 7Li(p,n)7Be reaction, Phys. Rev. C 85 (5) (2012). 055809-1-8.

[40] J. Praena, P.F. Mastinu, G. Martín Hernández, A method to obtain a Maxwell-Boltzmann neutron spectrum at kT=30 keV for nuclear astrophysics studies, in: Publ. Astron. Soc. Aust. 3 (26) (2009) 231–335.

[41] P.F. Mastinu, G. Martín Hernández, J. Praena, A method to obtain a Maxwell–Boltzmann neutron spectrum at kT=30 keV for nuclear astrophysics studies, Nucl. Instrum. Methods A 601 (2009) 333–338.